

Article

The Early Allometric Growth and Osteological Ontogeny of Pot-Bellied Seahorse (*Hippocampus abdominalis*, L. 1827) under Mass-Scale Captive Breeding Conditions in North China

Xuehui Shi ^{1,2}, Xinyi Tang ^{3,4}, Yichao Zhang ^{2,3}, Wenqi Wang ², Siyong Qin ⁵, Qinghua Liu ^{3,4,6,*}  and Jie Mei ^{1,*}¹ College of Fisheries, Huazhong Agricultural University, Wuhan 430070, China; xhshi@qau.edu.cn² School of Marine Science and Engineering, Qingdao Agricultural University, Qingdao 266109, China; 15293184681@163.com (Y.Z.); wenqi31@163.com (W.W.)³ CAS and Shandong Province Key Laboratory of Experimental Marine Biology, Institute of Oceanology, Chinese Academy of Sciences, Qingdao 266003, China⁴ Laboratory for Marine Biology and Biotechnology, Qingdao National Laboratory for Marine Science and Technology, Qingdao 266005, China⁵ Rizhao Duobao Aquaculture Co. Ltd., Rizhao 276800, China; taobaoyuye@126.com⁶ Key Laboratory of Breeding Biotechnology and Sustainable Aquaculture, Chinese Academy of Sciences, Wuhan 430072, China

* Correspondence: qinghualiu@qdio.ac.cn (Q.L.); jmei@mail.hzau.edu.cn (J.M.)

Abstract: Seahorses are valuable species for their use in traditional Chinese medicine, as well as for the aquarium trade as ornamentals and curiosities. To balance market demand and reduce pressure on wild populations, many countries have undertaken commercial seahorse cultivation. Skeletal development plays a crucial role in fish fry culture, affecting external morphology, feeding, and movement. This study investigated the ontogeny allometry, timing, and progression of skeletal development in *H. abdominalis* from DAB (day after birth) 1 to DAB 100 under mass-scale captive breeding conditions in north China. The results of this study revealed the growth rate was significantly increased between DAB 30 and DAB 54. Allometry analysis revealed that in the early stage, the head, trunk, and tail demonstrated almost isometric growth. However, in the later stage, the head and trunk exhibited negative isometric growth, whereas the tail displayed positive isometric growth. Skeletal staining results showed that newborn seahorses do not have ossified bones until DAB 11 (SL 28.14 ± 2.94 mm). Ossification was primarily observed in the jaw region and the tubular nasal structure of the cranium, which indicated the importance of the early development of feeding organs. The initial formation of ossified vertebral columns was observed at DAB 13 (SL 26.48 ± 0.63 mm), with the complete ossification of all vertebrae occurring by DAB 45 (SL 54.87 ± 4.70 mm). Furthermore, the cranium, rings, and plates were all fully ossified by DAB 30. Ossification of the fins began at DAB 23 (SL 31.27 ± 4.05 mm). However, neither of them were fully ossified by DAB 100. The pelvic fin and the complete structure of the caudal fin were not observed, possibly because of caudal fin ray structure degeneration within the pouch. In addition, no skeletal deformities were observed in all the tested samples. The results of this study provide valuable information on the developmental biology of *H. abdominalis*, enriching our understanding of their growth and offering insights for optimizing fish fry breeding technologies.

Keywords: seahorses; skeletal development; captive breeding; ossification; growth

Key Contribution: The findings of this study reveal a significant growth period spanning from DAB 30 to DAB 54, highlighting the importance of early ossification in the development of feeding organs. This finding provides valuable insights into the developmental biology of this species, with potential implications for the improvement of fish fry breeding techniques.



Citation: Shi, X.; Tang, X.; Zhang, Y.; Wang, W.; Qin, S.; Liu, Q.; Mei, J. The Early Allometric Growth and Osteological Ontogeny of Pot-Bellied Seahorse (*Hippocampus abdominalis*, L. 1827) under Mass-Scale Captive Breeding Conditions in North China. *Fishes* **2023**, *8*, 604. <https://doi.org/10.3390/fishes8120604>

Academic Editor: Giorgos Koumoundouros

Received: 12 October 2023
Revised: 20 November 2023
Accepted: 30 November 2023
Published: 8 December 2023



Copyright: © 2023 by the authors. Licensee MDPI, Basel, Switzerland. This article is an open access article distributed under the terms and conditions of the Creative Commons Attribution (CC BY) license (<https://creativecommons.org/licenses/by/4.0/>).

1. Introduction

Seahorses (*Hippocampus*) hold significant value due to their utilization in traditional Chinese medicine, as well as their popularity in the aquarium trade for their ornamental appeal and curiosity-inducing characteristics. Unfortunately, wild seahorse populations have faced threats from unsustainable fishing practices, environmental pollution, and the impacts of global climate change [1–4]. Recognizing the urgency of the situation, the international community took a crucial step in 2002 when seahorses became the first marine fishes to be regulated by CITES (Convention on International Trade in Endangered Species of Wild Fauna and Flora). By 2004, the majority of seahorse species worldwide had been included in Appendix II of CITES, marking a concerted effort to address the conservation challenges faced by these unique marine creatures [5].

To address the issue of unsustainable seahorse trade, captive rearing has emerged as a remedial practice [6,7]. Cultivating seahorses not only serves as an additional means to conserve these creatures but also helps reduce the strain on wild seahorse populations, offering alternative sources of income for farmers and fishers. Currently, *H. reidi* (Ginsburg, 1933), lined seahorse (*H. erectus*), three-spot seahorse (*H. trimaculatus*, Leach, 1814), and *H. kuda* (Bleeker, 1852) are the most popular culture species. The pot-bellied seahorse (*H. abdominalis*, Lesson, 1827), the largest of the seahorse species, is primarily found in the Southwest Pacific area, including Australia and New Zealand. It was introduced to China in 2016, and successful artificial breeding was achieved in 2020 [8]. While numerous studies focus on hippocampus species, the persistently low survival rate of juveniles remains a critical bottleneck in the sustainable development of the seahorse aquaculture industry [6,9].

The high mortality rate of juvenile seahorses is the main reason for limiting seahorse captivity. In recent years, studies conducted on light intensity [10,11], salinity [10,12,13], disease [14,15], and feeding [16–20] have become more frequent, improving the increased survival of juvenile seahorses. However, as of now, feed remains a critical factor limiting seahorse survival rates. The timing [17–19], type [20–22], size, and density [23] of feed are crucial for the growth of juvenile seahorses, and there is currently a lack of precise feeding strategies for juvenile seahorses.

The seahorse is a suction feeder, and the ingestion of food comprises preparation, expansion, and recovery phases. Skeletal development plays a crucial role in fish fry production, as it is closely correlated with essential aspects such as feeding, movement, and overall growth [24,25]. Therefore, investigating the characteristics of early seahorse skeletal development and determining the ossification patterns of elements related to feeding and movement are crucial for the precision cultivation of juvenile seahorses. For seahorses, previous studies usually focused on the growth, evolution, and brood pouch structure, with less research on early skeletal development and growth patterns. Additionally, the seahorse's skeleton is a modified bone structure with increased ossification compared to other bony fishes, which hold significant ornamental and medicinal value. Therefore, ensuring the proper skeleton development is crucial for cultivating a healthy seahorse. This study aims to investigate the growth characteristics, ossification, and morphological changes in *H. abdominalis*, including the timing and progression of skeletal development during DAB 0–100.

2. Materials and Methods

2.1. Rearing Conditions for Experimental Animal

Experimental animals were maintained under culture conditions in Rizhao, Shandong Province, China. The newborns were reared in 0.5-ton tanks (cylindrical, $r = 0.5$ m, $h = 0.65$ m) until DAB 30 and were transferred into 25-ton cement tanks (25 m \times 25 m \times 1 m). The tanks were cleaned every two days. The culture conditions were as follows: light intensity 2800 ± 500 lux, salinity 25‰, 16–21 °C, light: dark = 15:9, and constant aeration provided. The broodstock was fed frozen *Macrobranchium nipponense* cubes three times a day. After release, from DAB 1 to DBA 60, the larvae were fed fresh *Artemia salina*, *Copepods* from DAB 61 to DAB 90 and frozen *Mysis shrimp* from DAB 91 to DAB 100.

2.2. Sampling and Skeletal Staining

Approximately 20–25 individuals were sampled daily up to DAB 10, every 2 days until DAB 27, and subsequently every 7 days until DAB 100 for growth parameter analysis. Additionally, samples were taken every two days from DAB 1 to DAB 45 and every ten days from DAB 50 to DAB 80 for skeleton development analysis. The specimens were euthanized with a 0.05% solution MS-222 (Sigma-Aldrich, Saint Louis, FL, USA), fixed with 15% neutral buffered formalin for at least 48 h to ensure complete fixation, and then rinsed with distilled water for at least 2 days to wash away the formalin. Cartilage and bones were processed following the staining techniques established by Taylor and Van Dyke (1985) [26] and Digerkus and Uhler (1977) [27]. Finally, wash samples with potassium hydroxide (0.089 mol L^{-1}) and hydrogen peroxide (0.029 mol L^{-1}) solution 1:160 until the pigment disappears. The definition of bones and cartilages follows, provided by several authors: Gregory (1959), Azzarello (1989,1990) [28], Silveira (2000) [29], Arratia (2001) [30], Bruner (2008) [31], Leysen (2010, 2011) [32,33], and Novelli (2017) [34].

2.3. Observations and Measurements

The samples were placed in a vitreous petri dish, which contained glycerol. Thereafter, images were captured using a Nikon SMZ 1000 anatomical lens equipped with a Nikon DS-Fi1 imaging system (Nikon Instruments Inc., Japan). Photographs were edited using Adobe Photoshop 2023. The head length, trunk length, tail length, and standard length were measured by Digimizer (<https://www.digimizer.com/>).

2.4. Statistical Analysis

The calculation method of allometric growth was calculated with the power function $y = ax^b$ (Fuiman, 1983) [35], which is divided into positive allometric growth ($b > 1$), isometric growth ($b = 1$) and negative allometry growth ($b < 1$).

The calculation method of the absolute growth rate (AGR) was calculated using the equation $(L_f - L_i)/(t_2 - t_1)$ (Hopkins, 1992), L_f being the mean standard length (mm) of the sample at the end of each developmental stage at time t_2 and L_i being the mean standard length (mm) at the end of the previous stage at the time t_1 .

All data were statistically analyzed using SPSS Statistics 26 software (SPSS Inc., Chicago, IL, USA). The statistical data were presented as mean \pm S.D. The comparison of results was conducted with an analysis of variance followed by Tukey's test when significant variation was observed at the confidence level of 0.05.

3. Results

3.1. Allometric Growth

The growth performance of the juvenile *H. abdominalis* after being released from the brood pouch is shown in Table 1 and Figure 1. Two inflection points were observed from DAB 1 to DAB 100 (Figure 1a). Initially, the newborns exhibited a slow growth rate, while from DAB 30 to DAB 54, the growth rate significantly increased ($p < 0.05$) (Table 1). Cranium measurements showed approximating isometric growth during the early stage, followed by negative allometric growth in the later stage (Figure 1b). Similar changes were observed in the trunk (Figure 1c). Notably, the tail showed negative allometric growth in the early stage but transitioned to positive allometric growth in the later stage (Figure 1d).

Table 1. Growth of *H. abdominalis* during the development.

Growth	AGR (mm/day)
DAB	SL
1–30	0.58 ± 0.02^b
30–54	1.4 ± 0.01^a
54–100	0.17 ± 0.07^c

AGR—absolute growth rate, DAB—day after birth, SL—standard length. Values with different subscripts are significantly different ($p < 0.05$).

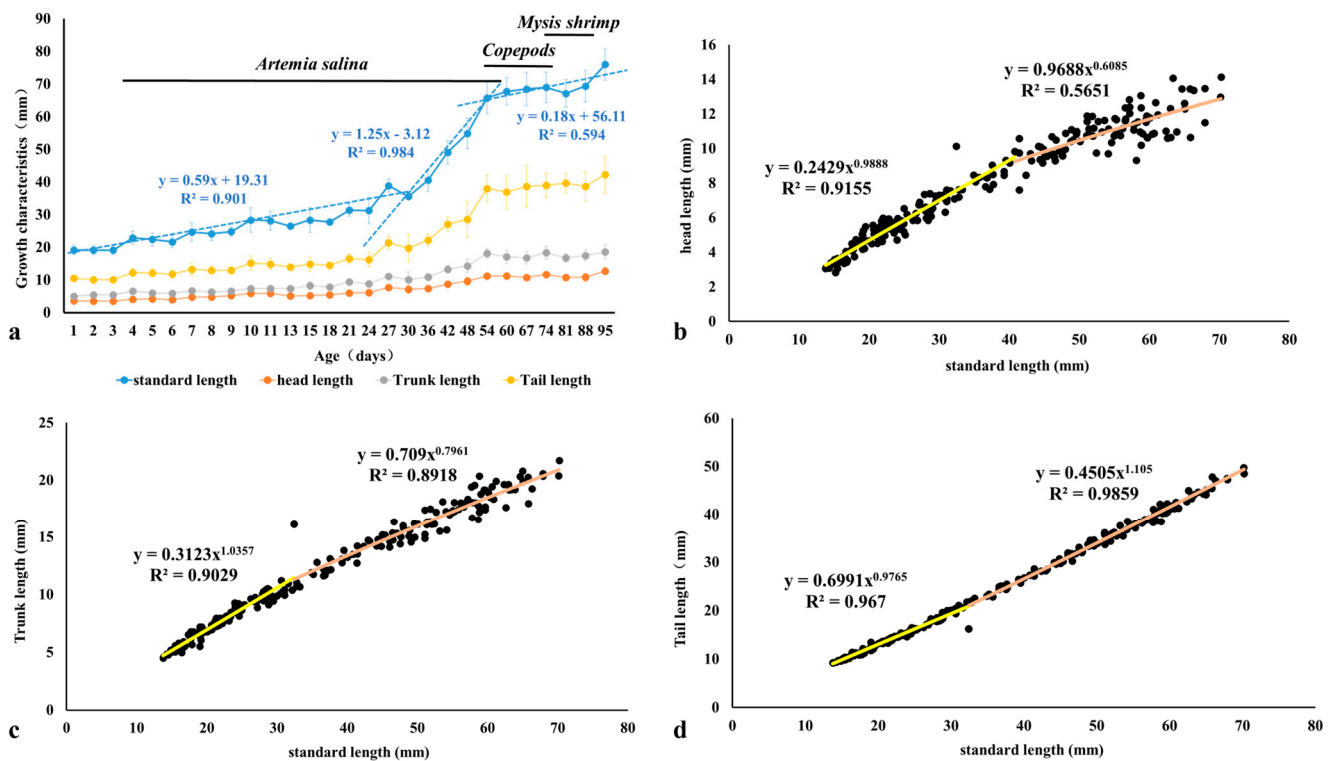


Figure 1. Growth and allometric growth characteristics of *H. abdominalis* from DAB 1 to DAB 100. (a) Growth characteristics related to days; (b) allometric growth characteristics between head length and standard length; (c) allometric growth characteristics between trunk length and standard length; (d) allometric growth characteristics between tail length and standard length. In Figure 1b–d, the two different colors of lines on each chart represent trend lines for distinct segments.

3.2. Timing and Progression of Skeletal Development

3.2.1. Timing and Progression of Cranium Development

The timing and progression of cranium development are shown in Figure 2a–n and Table 2.

- (1) DAB 1–7 (SL 19.21 ± 1.43 mm to SL 24.68 ± 2.86 mm; Figure 2a–c)

When newborns left the brood pouch, signs of chondrification were observed at the jaws, ethmoidal, orbital, hyoid, opercular, and neurocranium regions, except the parasphenoid bone exhibiting a slight degree of ossification at DAB 7.

- (2) DAB 8–11 (SL 24.16 ± 2.07 to SL 28.14 ± 2.94 mm; Figure 2d)

In the suspensoria, the hyomandibular cartilage showed signs of mineralization, resulting in the formation of two bones, the symplectic and the hyomandibular, in its anterior and posterior portions, respectively. In the jaw region, more pronounced chondrogenesis was observed in the dentary, retroarticular, and quadrate bones, as well as the rostral cartilage and palatine. The metapterygoid bone began chondrification. In the neurocranium, the basioccipital bone located in the upper opercular region displayed partial ossification.

- (3) DAB 12–13 (SL 26.48 ± 0.63 mm; Figure 2e)

In the lower jaw, the dentary bone, as well as the retroarticular bone and quadrate, were in an early stage of ossification. The hyomandibular and symplectic bones fused together to form a thin bone, which extended from the posterior part of the jaw region to underneath the orbital region. The opercular region remained cartilaginous, while in the hyoid region, the ceratohyal and hypohyal bones began the process of ossification. The pre-coronet spine located in the upper portion of the neurocranium exhibited partial ossification.

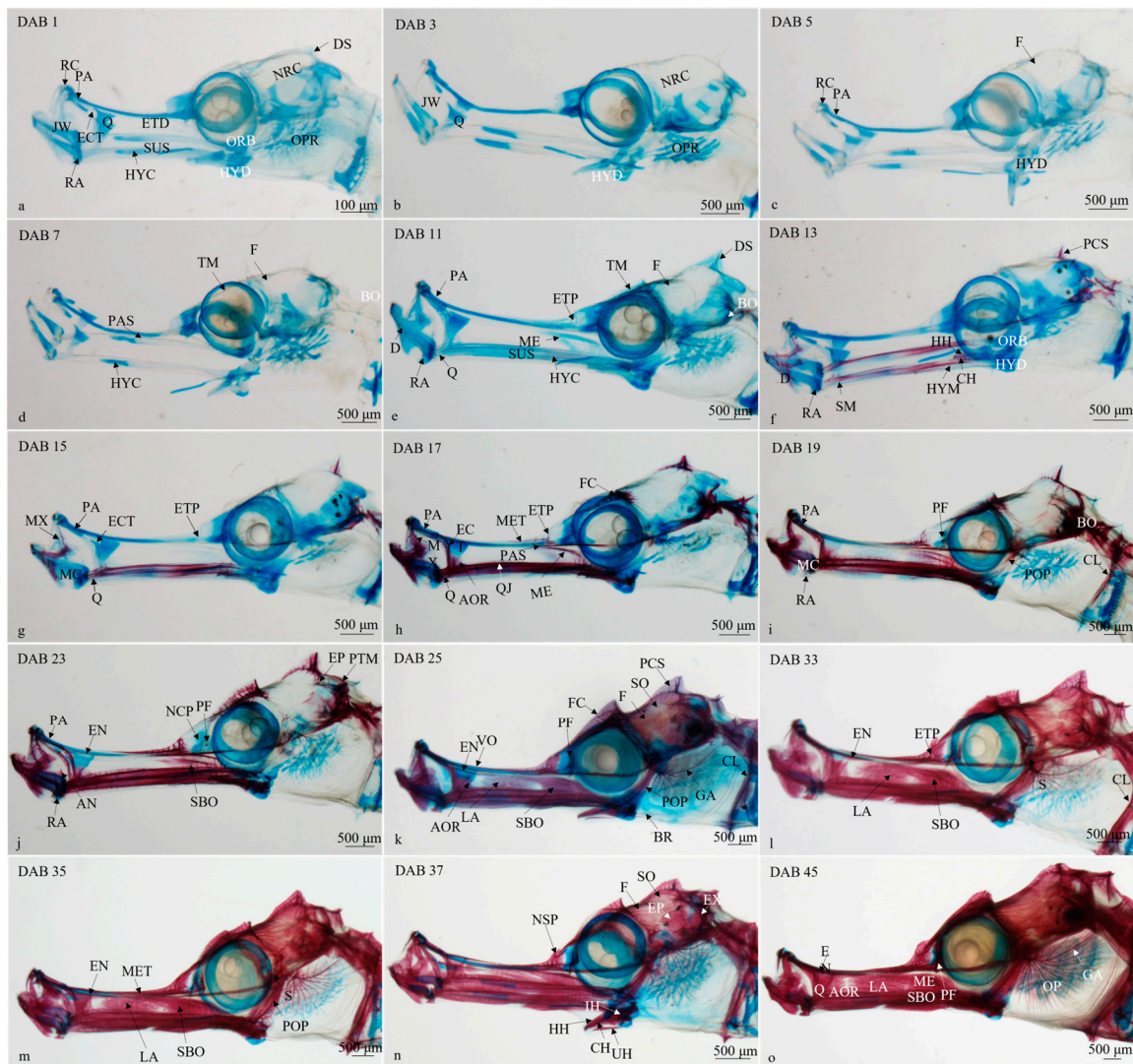


Figure 2. Osteological development of *H. abdominalis* cranium (DAB 1–DAB 45). Head, lateral view (a–o). AN—angular, AOR—antorbital, BO—basioccipital, BR—branchiostegal rays, CH—ceratohyal, CL—cleithrum, D—dentary, DS—dermal substance, ECT—ectopterygoid, EN—endopterygoid, EP—epiotics, ETD—ethmoidal region, ETP—ethmoid plate, EX—exoccipitals, F—frontal, FC—frontal crest, GA—gill arc, HH—hypohyal, HYC—hyomandibular cartilage, HYD—hyoid region, HYM—hyomandibular, IH—interhyal, JW—jaw region, LA—lachrymal, MC—Meckel’s cartilage, ME—metapterygoid, MET—mesethmoid, MX—maxillary, NCP—nasal capsule, NRC—neurocranium, OP—operculum, OPR—opercular region, ORB—orbital region, PA—palatine, PAS—parasphenoid, PCS—pre-coronet spine, PF—pre-frontal, PM—pre-maxillary, POP—pre-opercular, PTM—post-temporal, Q—quadrate, QJ—quadratojugal, RA—retroarticular, RC—rostral cartilage, S—sphenotic, SBO—sub-orbital, SM—symplectic, SUS—suspensoria, TM—taenia marginalis, UH—urohyal. Scale bar: 100 µm (a), scale bar: 500 µm (b–o).

Table 2. Osteological development of cranium in *H. abdominalis* (DAB 1–DAB 75). TABLE was made based on the ossification nodes; unobserved cartilage is white, blue means element in cartilaginous state, red means element in ossified state, and the light red means element in incomplete ossification stage.

Skeletal Elements	Time (DAB)															
	3	7	11	15	19	23	27	31	35	39	41	45	55	65	75	
Branchiocranium																
Angular																
Antorbital																
Cleithrum																
Dentary																
Ectopterygoid																
Endopterygoid																
Ethmoid plate																
Hyomandibular																
Lachrymal																
Maxillary																
Meckel's cartilage																
Mesethmoid																
Metapterygoid																
Nasal spine																
Operculum																
Palatine																
Parasphenoid																
Quadrate																
Retroarticular																
Rostral cartilage																
Sub-orbital																
Symplectic																
Vomer																
Neurocranium																
Basioccipital																
Coronet																
Epiotic																
Exoccipital																
Frontal																
Frontal crests																
Post-temporal																
Precoronet spine																
Sphenotic																
Supra-occipital																
Legend	Absence			Cartilage				Cartilage-bone				bone				

(4) DAB 14–17 (SL 28.34 ± 3.87 mm; Figure 2f,g)

There was an increase in the size of the quadrate. In the upper jaw, ossification of the ectopterygoid and maxillary bones were observed. The zone standing over the quadratojugal bone was composed of three bones, namely, the antorbital bone, the lachrymal bone, and the sub-orbital bone, with the antorbital bone showing signs of mineralization. In the ethmoidal region, the mesethmoid bone ossified. The frontal bone expanded and extended above the otic capsule, forming a frontal crest. The parasphenoid bone extended from the orbital region to the jaw and basioccipital directions. The metapterygoid bone was partially ossified.

(5) DAB 18–23 (SL 27.76 ± 0.80 to SL 31.27 ± 4.05 mm; Figure 2h,i)

The Meckel's cartilage was covered by a dermal ossification. The retroarticular bone mineralization was more obvious, and the palatine bone showed significant ossification. The angular bone located in the posterior portion of the Meckel's cartilage displayed partial ossification. The sub-orbital bone started to ossify, while the endopterygoid bone still remained cartilaginous. There was an increased mineralization in the nasal capsule region. The prefrontal bone, located between the eye socket and nasal capsule, started to ossify. The post-temporal and epiotic bones, as well as the pre-opercular bone, showed ossification.

(6) DAB 24–25 (SL 31.27 ± 1.93 mm; Figure 2j)

The mineralization of antorbital, lachrymal, and sub-orbital bones exhibited more pronounced mineralization. The vomer bone initiated the process of ossification. The ossification in the prefrontal bone increased. The supra-occipital bone underwent ossification, forming a thin bone lamina that covered the upper portion of the neurocranium. The frontal crest and pre-coronet spine were completely ossified. In the opercular region, the branchiostegal rays and gill arches display partial ossification. The cleithrum bone, located in the posterior portion of the opercular region, showed significant ossification.

(7) DAB 26–35 (SL 38.89 ± 1.98 to SL 40.55 ± 3.33 mm; Figure 2k,l)

At DAB 33, the ethmoidal plate and the cleithrum bone were completely ossified, while the sphenotic bone started to ossify. The endopterygoid bone extended from the jaws region to the nasal capsule region was partially ossified. Until DAB 35, both the jaw region and pre-opercular bone were at an advanced stage of ossification. The lachrymal bone started to fuse with the sub-orbital bone.

(8) DAB 36–45 (SL 49.14 ± 3.53 to SL 54.87 ± 4.70 mm; Figure 2m,n)

At DAB 37, The neurocranium and the nasal capsule regions were at an advanced stage of ossification. Until DAB 45, ossification in the opercular region became visible, specifically in the operculum, which covered the already ossified gill arches. The bones that comprise the lateral face of the snout, including the quadrate, endopterygoid, lachrymal, antorbital, and sub-orbital bones, gradually fused together, forming a laminar ossified area. The cranium was basically completely ossified.

3.2.2. Timing and Progression of Coronet Development

The timing and progression of coronet development are shown in Figure 3a–j and Table 2. Newborns showed dermal substance, which was located in the upper head (Figure 3a). There were no traces of ossification in the coronet (Figure 3a–c). The post-temporal bone located in the posterior portion of the supra-occipital bone and underneath the coronet did not have any mineralization until DAB 11 (Figure 3c). At DAB 13, the pre-coronet spine was partially ossified (Figure 3d). The coronet started to ossify at DAB 21 (Figure 3f), and the pre-coronet spine reached an advanced stage of ossification at DAB 25 (Figure 3g). Until DAB 45, the pre-coronet spine, coronet, supra-occipital, and post-temporal bones were completely ossified (Figure 3j).

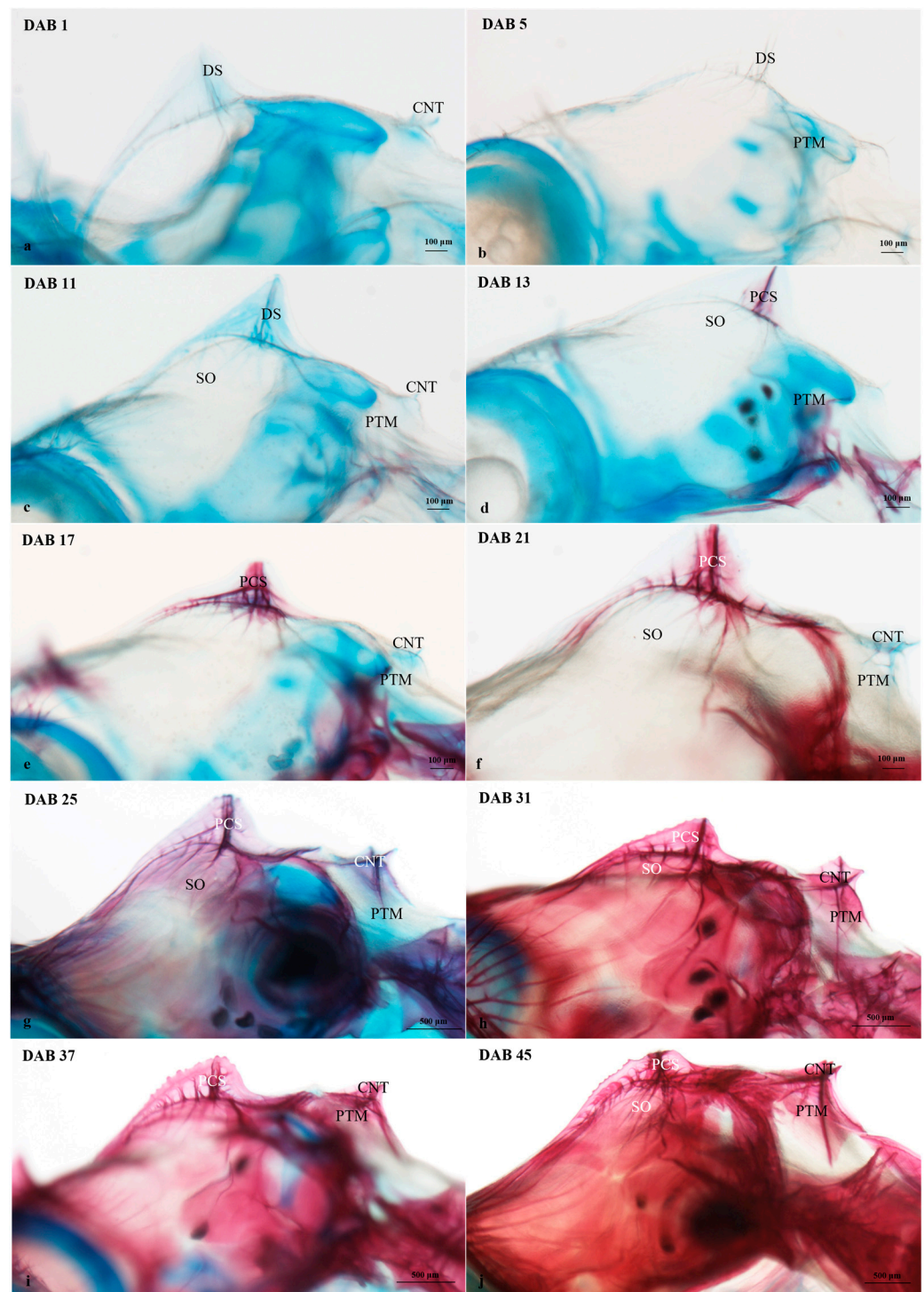


Figure 3. Osteological development of *H. abdominalis* neurocranium and coronet (DAB 1–DAB 45). Head, lateral view (a–j). CNT—coronet, DS—dermal substance, PCS—pre-coronet spine, PTM—post temporal, SO—supraoccipital. Scale bar: 100 µm (a–f), scale bar: 500 µm (g–j).

3.2.3. Timing and Progression of Vertebral Column Development

The timing and progression of vertebral column development are shown in Figure 4a–j and Table 3.

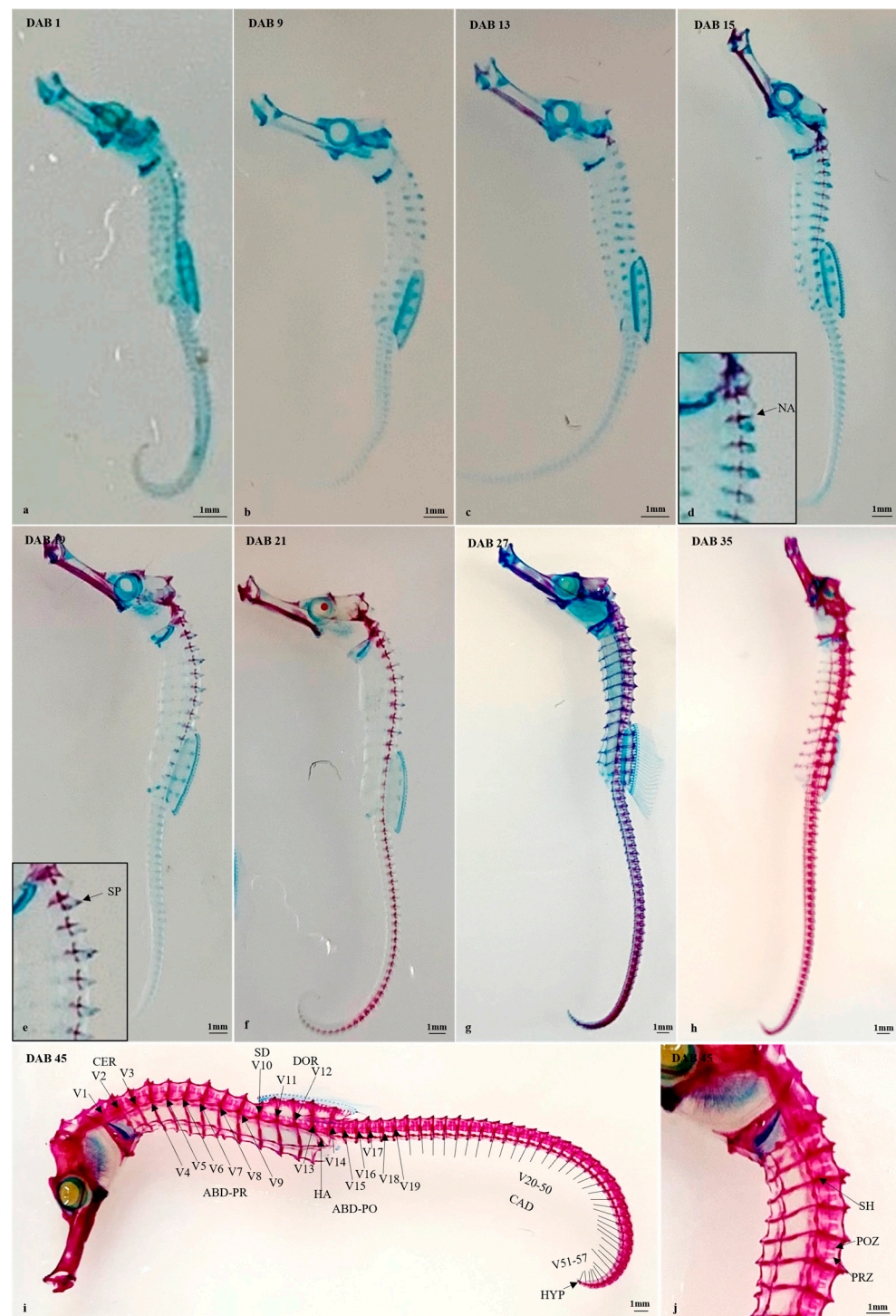


Figure 4. Osteological development of *H. abdominalis* axial skeleton (DAB 1–DAB 45). Vertebral system, lateral view (a–j). ABD-PR—abdominal pre-dorsal vertebrae, ABD-PO—abdominal post-dorsal vertebrae, CAD—caudal vertebrae, CER—cervical vertebrae, DOR—dorsal vertebrae, HA—haemal arch, HYP—hypural plate, NA—neural arch, POZ—postzygapophysis, PRZ—prezygapophysis, SD—supra-dorsal vertebra, SH—shield, V—vertebra. Scale bar: 1 mm.

Table 3. Osteological development of vertebral column in *H. abdominalis* (DAB 1–DAB 75). TABLE was made based on the ossification nodes; unobserved cartilage is white, blue means element in cartilaginous state, red means element in ossified state, and the light red means element in incomplete ossification stage.

Skeletal Elements	Time (DAB)															
	3	7	11	15	19	23	27	31	35	39	41	45	55	65	75	
Axial skeleton/shields																
Abdominal pre-dorsal vertebrae	Blue		Light Red			Red										
Abdominal post-dorsal vertebrae	Blue				Light Red			Red								
Caudal vertebrae	Blue					Light Red		Red								
cervical vertebrae	Blue		Light Red			Red										
Dermal body plates	Blue	Light Red							Red							
Dorsal vertebrae	Blue				Light Red		Red									
Haemal arch	Blue										Light Red			Red		
Hypural plate	Blue								Light Red							Red
Neural arch	Blue				Light Red				Red							
Post-zygapophysis	Absence		Blue		Light Red		Red									
Pre-zygapophysis	Absence		Blue		Light Red		Red									
Shields	Absence		Blue		Light Red				Red							
Legend	Absence		Cartilage				Cartilage-bone				bone					
			Blue				Light Red				Red					

The armor consisting of the vertebral system, spine, shield, and plate provided protection for the seahorse. Initially, the vertebral system showed no signs of mineralization in DAB1–9 (Figure 4a,b). By DAB 13, the ossification of the cranium was evident (Figure 4c). At DAB 15, the cervical, abdominal, and supra-dorsal vertebrae started to ossify (Figure 4d). Signs of ossification were observed in the neural arch of V1 and V2. The spine, which was located in the upper part of the V2, was partially ossified at DAB 19 (Figure 4e). At DAB 21, the abdominal, dorsal, and caudal vertebrae started to mineralize (Figure 4f). DAB 22–44, ossification of shields progressed along the entire body, forming rings along the transverse axis of the body (Figure 4g–j). The postzygapophysis and the prezygapophysis, paired pointed apophysis located on both sides of the neural arch, exhibited mineralization (Figure 4j). The haemal arch supporting the anal fin, which was present in V13, displayed noticeable ossification (Figure 4i). By DAB 45, the vertebral system was completely ossified (Figure 4i,j).

3.2.4. Timing and Progression of Fin Development

The timing and progression of fin development are shown in Figures 5–7 and Table 4.

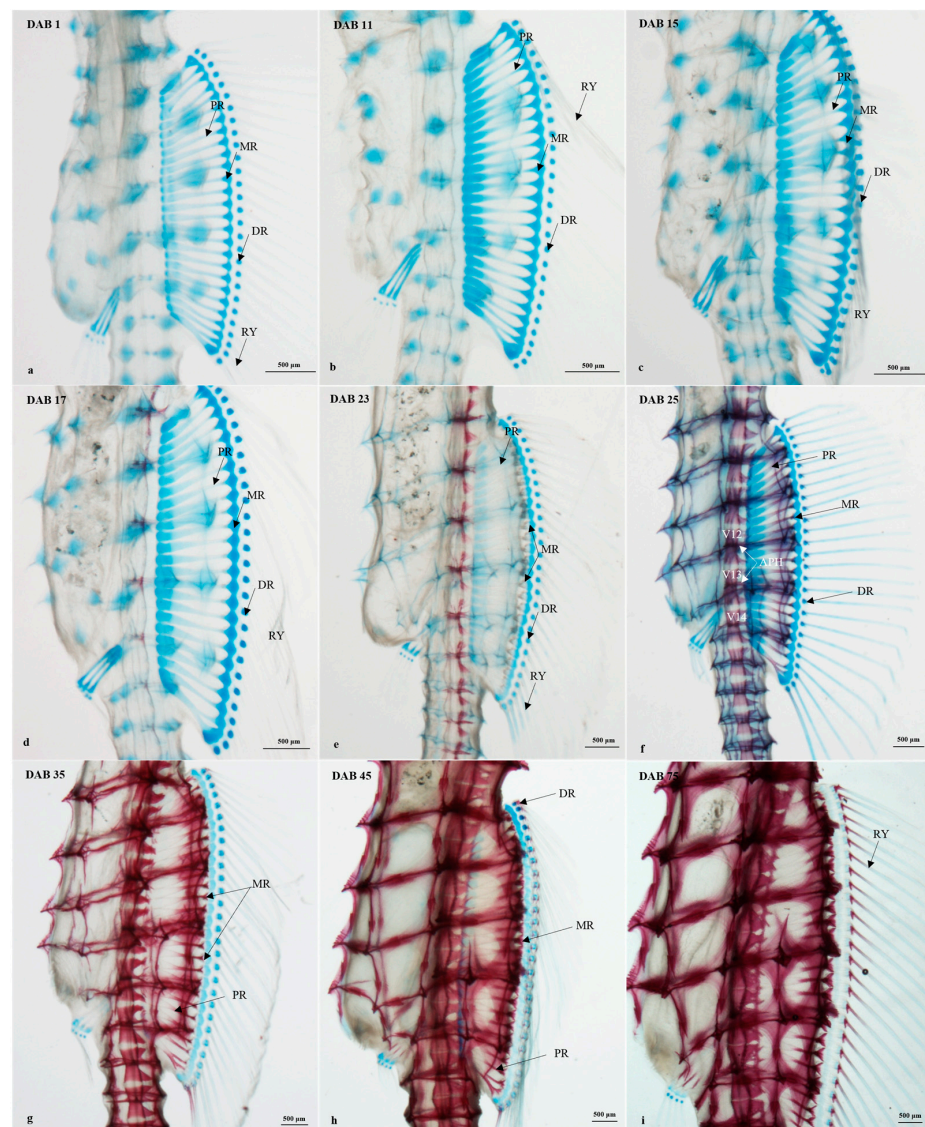


Figure 5. Osteological development of *H. abdominalis* appendicular skeleton (DAB 1–DAB 70). Dorsal fin, lateral view (a–i). APH—apophysis, DR—distal radial, MR—medial radial, PR—proximal radial, RY—rays, V—vertebra. Scale bar: 500 µm.

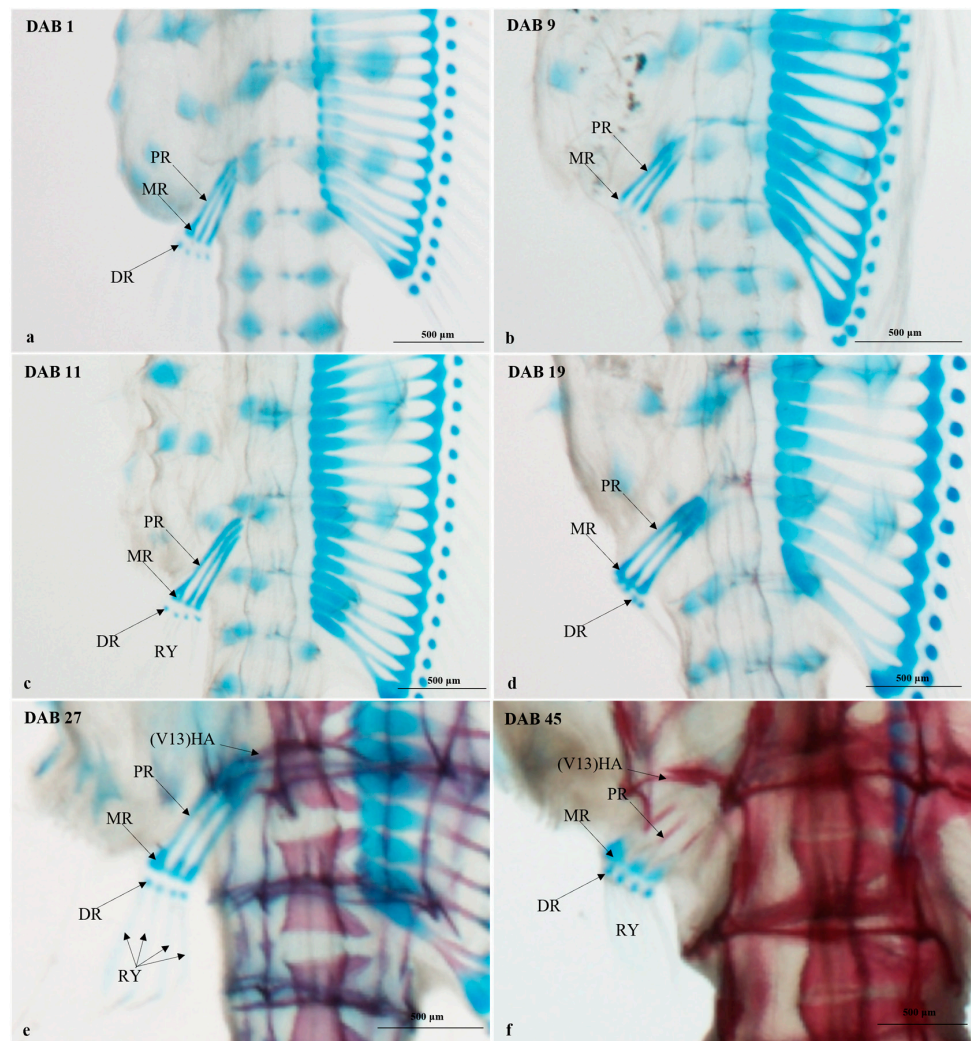


Figure 6. Osteological development of *H. abdominalis* appendicular skeleton (DAB–DAB 45). Anal fin, lateral view (a–f). DR—distal radial, HA—haemal arch, MR—medial radial, PR—proximal radial, RY—rays, V—vertebra. Scale bar: 500 µm.

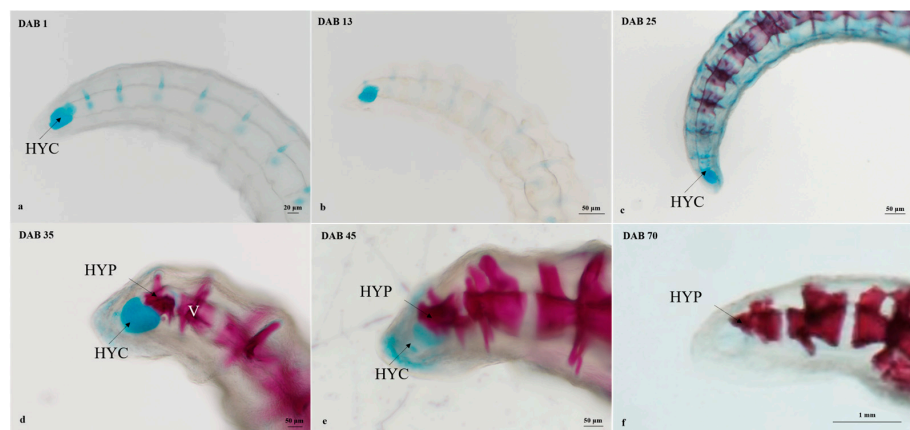


Figure 7. Osteological development of *H. abdominalis* appendicular skeleton (DAB 1–DAB 70). Caudal fin, lateral view (a–f). HYC—hypural cartilage, HYP—hypural plate, V—vertebra. Scale bar: 20 µm (a), scale bar: 50 µm (b–e), scale bar: 1 mm (f).

Table 4. Osteological development of appendicular skeleton in *H. abdominalis* (DAB 1–DAB 75). TABLE was made based on the ossification nodes; unobserved cartilage is white, blue means element in cartilaginous state, red means element in ossified state, and the light red means element in incomplete ossification stage.

Skeletal Elements		Time (DAB)													
		3	7	11	15	19	23	27	31	35	39	41	45	55	65
Appendicular skeleton															
Distal radial	anal fin	[Blue bar]													
	dorsal fin	[Blue bar]													
	Caudal fin	[Blue bar until 35] [Light red bar until 65] [Red bar until 75]													
Medial radial	anal fin	[Blue bar]													
	dorsal fin	[Blue bar until 23] [Light red bar until 35] [Red bar until 75]													
	Caudal fin	[White bar]													
Proximal radial	anal fin	[Blue bar]													
	dorsal fin	[Blue bar until 39] [Light red bar until 45] [Red bar until 75]													
	Caudal fin	[White bar]													
ray	anal fin	[Blue bar]													
	dorsal fin	[White bar until 7] [Blue bar until 45] [Light red bar until 65] [Red bar until 75]													
	Caudal fin	[White bar]													
Legend		Absence				Cartilage				Cartilage-bone				bone	
		[White bar]				[Blue bar]				[Light red bar]				[Red bar]	

Dorsal fin (Figure 5a–i)

No ossification was observed in the dorsal fin (27 rays) of the newborns (Figure 5a). The proximal radials, medial radials, distal radials, and rays were still in cartilage status and clearly visible (Figure 5b–d). Following ossification in the vertebral centrum, the proximal radials started to ossify (Figure 5e,f). At DAB 25, the proximal radials were partially ossified, while the distal radials started to ossify (Figure 5g). The bifurcated apophysis, which supported the dorsal fin, was present on V12, V13, and V14. At DAB 35, the rays started to ossify (Figure 5g). By DAB 45, the ossification of the proximal radials and the distal radials became more obvious, and the ossified rays were present. At DAB 60, the ossification of the rays continued.

Anal fin (Figure 6a–f)

The structure of the anal fin was similar to that of the dorsal fin but smaller in size. After release, there were no signs of ossification in the three proximal radials, four distal radials, and four rays located near the anus (Figure 6a). The ossified proximal radials extending from the haemal arch to the medial radials were observed at DAB 45 (Figure 6f).

Caudal fin (Figure 7a–f)

The rays were not present in newborns (Figure 7a). The hypural plate was formed by the ossification of the hypural cartilage, which is located in the most distal part of the spinal system. When newborns left the brood pouch, the hypural cartilage was already present, and it showed partial ossification (Figure 7b–e). By DAB 70, the caudal fin structure was completely ossified (Figure 7f).

4. Discussion

In certain species, newborns exhibit low feeding efficiency due to the incomplete development of organs for food ingestion and movement. During this stage, a significant portion of their energy is allocated to basal metabolism, leading to slow growth. However, as these organs mature in later stages, feeding efficiency increases, facilitating rapid growth [36].

During the experimental period from DAB 1 to DAB 27, the growth rate of *H. abdominalis* was initially slow, measuring 0.59 mm day^{-1} , but saw a significant increase to 1.25 mm day^{-1} by DAB 30. However, from DAB 54 onward, the growth rate declined to 0.18 mm day^{-1} . This observed pattern aligns with findings in other species, including *H. reidi* [37], *H. erectus* [38], *H. kuda* [39], *Scopthalmus maximus* [40], and *Oplegnathus fasciatus* [41].

Feeding efficiency is a critical determinant of larval fish survival rates. Consequently, organs associated with survival undergo preferential development to enhance overall survival, exhibiting an allometric growth pattern [35,42]. The development of the cranium, particularly in early developmental stages, is closely linked to functions like food ingestion and respiration [43]. In some species, such as *Epinephelus coioides* [44], *Scopthalmus maximus* [40], and *Oplegnathus punctatus* [45], the cranium displays positive allometric growth during early developmental stages. Similar patterns have been observed in seahorses like *H. erectus* [38]; however, the cranium of *H. kuda* [39] remains nearly isometric throughout the entire early developmental period. In our study, the cranium displayed nearly isometric growth during the earlier developmental stages and shifted to negative allometric growth in later stages. These results suggest that each teleost species exhibits a unique allometric growth pattern tailored to its development.

The skeletal system is crucial for most animals, providing structural support, safeguarding vital organs, and enabling movement. In seahorses, the process of ossification in newborns begins either inside or outside of the pouch. In this study, we observed that the ossification of *H. abdominalis* initiated outside the pouch at DAB 11, a pattern also noted in *H. reidi* (DAB 4), *H. erectus* (DAB 16), and *H. subelongatus* (DAB 4) [37]. However, the ossification of *H. zosterae* and *H. hippocampus* began within the pouch [34,37]. Franz-Odenaal [37] suggests that this difference in growth may be related to seahorse body size and evolutionary relationships. Overall, the diversity in the initiation of ossification processes among seahorse species underscores the complexity of their skeletal development, potentially influenced by factors such as body size and evolutionary history.

The hippocampus species are known as extreme predators because of their tubular nasal structure, which is extremely capable of feeding [24,33,46]. During the early embryonic period stage, this tubular nose undergoes transforms from folding elongation [28], coinciding with the gradual elongation of the ethmoid region. This distinctive nasal structure facilitates a specialized feeding technique called pivot feeding, relying on the coordinated movement of four integrated parts: the neurocranium, lower jaws, hyoid, and snout [47]. The jaws are connected to the neurocranium and hyoid by the hyomandibular and symplectic bones. Intriguingly, our study revealed that the jaw region, hyoid region, and suspensoria exhibited the earliest signs of ossification. Similar observations have been made in other seahorse species, such as *H. subelongatus* [37] and *H. hippocampus* [34] suspensoria, which exhibited the earliest signs of ossification. Similar observations have been made in other seahorse species, such as *H. subelongatus* [37] and *H. hippocampus* [34], underscoring the vital roles of these structures during the early stages of hippocampus development.

Seahorses exhibit a certain selectivity in prey size during feeding, typically opting for the largest prey they can capture, a behavior that may be correlated with the matching of their snout width to the body width of the prey [17,48]. This study documents the developmental process of the tubular nasal structure in *H. abdominalis*, providing a foundational theoretical basis for accurately calculating the size of prey to be fed. With an increase in snout depth and length, larvae seahorses may have been able to select larger prey [10,17,23,49]. This study reveals that at DAB 30, elements related to seahorse feeding are fully ossified, accompanied by a significant increase in growth rate. This highlights the importance of complete ossification for their feeding, suggesting that increasing feed density and size after DAB 30 may contribute to higher survival rates in juvenile seahorses.

In general, seahorses typically display a range of tail rings between 34 and 39 in number and dorsal fin rays ranging from 15 to 20 [3]. However, *H. abdominalis* distinguishes itself from other species with its higher number of rings and rays. In our study, we noted that *H. abdominalis* exhibited 12–13 trunk rings, 45–46 tail rings, and 26–27 dorsal fin rays, consistent with the observations of Lourie [3]. This unique characteristic provides a rapid and distinctive means of identifying *H. abdominalis* compared to other seahorse species.

Seahorses stand out from the majority of other teleost fish due to a distinctive anatomical feature: instead of scales, they have body plates [50]. These plates are arranged in a square ring formed by four interconnected plates. This unique structure allows seahorses to flex their tails ventrally, using them as grasping and holding appendages for postural support [51]. Additionally, the presence of these body plates provides a degree of protection against vertebral fractures resulting from impacts and compressions [50,52].

5. Conclusions

During the initial 100 days of seahorse development, the growth rate of *H. abdominalis* exhibits a slow–fast–slow pattern, correlating with the incomplete maturation of feeding behavior and locomotor organs in juvenile seahorses. Notably, on DAB 30 of the experiment, a significant acceleration in seahorse growth rate is observed, concomitant with near-complete ossification. This suggests that augmenting feed density and individual size around this juncture may contribute positively to enhancing juvenile *H. abdominalis* survival rates.

Author Contributions: X.S. methodology; Q.L. conceptualization, writing—review and editing; X.T. experimental, writing—review and editing; Y.Z. methodology, validation; X.S. supervision and project administration; J.M., S.Q. and W.W. resource. All authors have read and agreed to the published version of the manuscript.

Funding: This work was supported by the Research and Development Program of Shandong Province (2021LZGC029), Shandong Province Natural Science Foundation (ZR2020KC038), and China Agriculture Research System (CARS-47-G21).

Institutional Review Board Statement: The study was conducted in accordance with the Declaration of Helsinki and approved by the Animal Protection and Utilization Committee of the Institute of Oceanography, Chinese Academy of Sciences (Approval Code: IOCAS20231010PPFA0008; Approval Date: 10 October 2023).

Data Availability Statement: Data are contained within the article.

Conflicts of Interest: I hereby declare that the work described in this article is original research, has not been previously published, and is not currently under consideration for publication elsewhere. Each author has reviewed and approved the content of the submitted manuscript and has agreed to be listed as an author. Furthermore, we confirm that there are no known competing financial interest or personal relationships that may have influenced the findings presented here.

References

1. Pan, J.; Marcoval, M.A.; Bazzini, S.M.; Vallina, M.V.; Marco, S.G.D. Coastal Marine Biodiversity: Challenges and Threats. In *Marine Ecology in a Changing World*; CRC Press: Boca Raton, FL, USA, 2013.
2. Woods, C.M.C. Improving initial survival in cultured seahorses, *Hippocampus abdominalis* Leeson, 1827 (Teleostei: Syngnathidae). *Aquaculture* **2000**, *190*, 377–388. [[CrossRef](#)]
3. Lourie, S.A.; Stanley, H.F.; Vincent, A.C.J.; Hall, H.J.; Pritchard, J.C.; Casey, S.P. *Seahorses: An Identification Guide to the World's Species and Their Conservation*; Project Seahorse: Vancouver, BC, Canada, 1999.
4. Job, S.D.; Do, H.H.; Meeuwig, J.J.; Hall, H.J. Culturing the oceanic seahorse, *Hippocampus kuda*. *Aquaculture* **2002**, *214*, 333–341. [[CrossRef](#)]
5. Johannesburg, A.C.o. Convention on international trade in endangered species of wild fauna and flora. *J. Int. Wildl. Law Policy* **2005**, *8*, 115–127.
6. Koldewey, H.J.; Martin-Smith, K.M. A global review of seahorse aquaculture. *Aquaculture* **2010**, *302*, 131–152. [[CrossRef](#)]
7. Cohen, F.P.A.; Valenti, W.C.; Planas, M.; Calado, R.J. Seahorse Aquaculture, Biology and Conservation: Knowledge Gaps and Research Opportunities. *Rev. Fish. Sci. Aquac.* **2016**, *25*, 100–111. [[CrossRef](#)]
8. He, L.; Jianfei, Q.; Lin, J.; Chen, X.; Luo, H.; Wang, Q.; Leyun, Z. Artificial propagation and seedling technique of *Hippocampus abdominalis*. *J. Appl. Oceanogr.* **2022**, *41*, 701–707.
9. Nur, F.A.H.; Christianus, A.; Abdullah, A.R.; Zakaria, M.H.; Saad, C.R. Effects of thyroxine, cod liver oil and potassium iodide on growth and survival of juvenile seahorse, *Hippocampus barbouri*. *Aquaculture* **2018**, *49*, 867–873. [[CrossRef](#)]
10. Murugan, A.; Dhanya, S.; Sreepada, R.A.; Rajagopal, S.; Balasubramanian, T. Breeding and mass-scale rearing of three spotted seahorse, *Hippocampus trimaculatus* Leach under captive conditions. *Aquaculture* **2009**, *290*, 87–96. [[CrossRef](#)]
11. Liu, X.; Zhang, D.; Lin, T.; Li, S. Culturing low quality juveniles of the lined seahorse, *Hippocampus erectus*. *Aquac. Res.* **2023**, *30*, 101561. [[CrossRef](#)]
12. Huang, J.; Qin, G.; Zhang, B.; Tan, S.; Sun, J.; Lin, Q. Effects of food, salinity, and ammonia-nitrogen on the physiology of juvenile seahorse (*Hippocampus erectus*) in two typical culture models in China. *Aquaculture* **2020**, *520*, 734965. [[CrossRef](#)]
13. Zhang, D.; Liu, X.; Lin, T.; Li, S.; Shen, F.; Wang, Y. Culturing the lined seahorse (*Hippocampus erectus*) in extensive shrimp ponds and cages. *J. World Aquac. Soc.* **2023**. [[CrossRef](#)]
14. Jiang, F.; Huang, H.; Yang, N.; Feng, H.; Li, Y.; Han, B. Isolation, identification, and biological control in vitro of tail rot pathogen strain from *Hippocampus kuda*. *PLoS ONE* **2020**, *15*, e0232162. [[CrossRef](#)] [[PubMed](#)]
15. Li, Y.; Wang, Z.; Zheng, F.; Wang, B.; Liu, H.; Zhang, P.; Xin, M. Identification and characterization of the pathogen associated with skin ulcer syndrome in lined seahorse *Hippocampus erectus*. *Aquac. Res.* **2019**, *51*, 989–999. [[CrossRef](#)]
16. Willadino, L.; Souza-Santos, L.P.; Mélo, R.C.S.; Brito, A.P.; Barros, N.C.S.; Araújo-Castro, C.M.V.; Galvão, D.B.; Gouveia, A.; Regis, C.G.; Cavalli, R.O. Ingestion rate, survival and growth of newly released seahorse *Hippocampus reidi* fed exclusively on cultured live food items. *Aquaculture* **2012**, *360–361*, 10–16. [[CrossRef](#)]
17. Celino, F.T.; Hilomen-Garcia, G.V.; del Norte-Campos, A.G.C. Feeding selectivity of the seahorse, *Hippocampus kuda* (Bleeker), juveniles under laboratory conditions. *Aquac. Res.* **2012**, *43*, 1804–1815. [[CrossRef](#)]
18. Otero-Ferrer, F.; Molina, L.; Socorro, J.; Herrera, R.; Fernández-Palacios, H.; Soledad Izquierdo, M. Live prey first feeding regimes for short-snouted seahorse *Hippocampus hippocampus* (Linnaeus, 1758) juveniles. *Aquac. Res.* **2010**, *41*, e8–e19. [[CrossRef](#)]
19. Vargas-Abúndez, J.A.; Simões, N.; Mascaró, M. Feeding the lined seahorse *Hippocampus erectus* with frozen amphipods. *Aquaculture* **2018**, *491*, 82–85. [[CrossRef](#)]
20. Schubert, P.; Vogt, L.; Eder, K.; Haufler, T.; Wilke, T. Effects of Feed Species and HUFA Composition on Survival and Growth of the Longsnout Seahorse (*Hippocampus reidi*). *Front. Mar. Sci.* **2016**, *3*, 53. [[CrossRef](#)]
21. Planas, M.; Olivotto, I.; González, M.J.; Laurà, R.; Angeletti, C.; Amici, A.; Zarantoniello, M. Pre-breeding Diets in the Seahorse *Hippocampus reidi*: How Do They Affect Fatty Acid Profiles, Energetic Status and Histological Features in Newborn? *Front. Mar. Sci.* **2021**, *8*, 58. [[CrossRef](#)]
22. Del Vecchio, G.; Otero-Ferrer, F.; Pascual, C.; Rosas, C.; Simoes, N.; Mascaró, M. Effect of starvation on survival and biochemical profile of newborn juvenile lined seahorses, *Hippocampus erectus* (Perry, 1810). *Aquac. Res.* **2019**, *50*, 3729–3740. [[CrossRef](#)]

23. Hora, M.d.S.C.d.; Joyeux, J.-C. Closing the reproductive cycle: Growth of the seahorse *Hippocampus reidi* (Teleostei, Syngnathidae) from birth to adulthood under experimental conditions. *Aquaculture* **2009**, *292*, 37–41. [[CrossRef](#)]
24. Avidan, C.; Day, S.W.; Holzman, R. A power amplification dyad in seahorses. *Proc. Biol. Sci.* **2023**, *290*, 20230520. [[CrossRef](#)] [[PubMed](#)]
25. Manning, C.G.; Foster, S.J.; Vincent, A.C.J. A review of the diets and feeding behaviours of a family of biologically diverse marine fishes (Family Syngnathidae). *Rev. Fish Biol. Fish.* **2019**, *29*, 197–221. [[CrossRef](#)]
26. Taylor, W.R.; Vandyke, G.C. Revised Procedures for Staining and Clearing Small Fishes and Other Vertebrates For Bone And Cartilage Study. *Cybium* **1985**, *9*, 107–119.
27. Dingerkus, G.; Uhler, L.D. Enzyme clearing of alcian blue stained whole small vertebrates for demonstration of cartilage. *Stain Technol.* **1977**, *52*, 229–232. [[CrossRef](#)] [[PubMed](#)]
28. Azzarello, M.Y. A Comparative Study of the Developmental Osteology of *Syngnathus scovelli* and *Hippocampus zosterae* (Pisces, Syngnathidae) and Its Phylogenetic Implications. Ph.D. Thesis, University of South Florida, St. Petersburg, FL, USA, 1990.
29. Silveira, R.B.J.Z. Desenvolvimento osteológico de *Hippocampus reidi* Ginsburg (Pisces, Syngnathiformes, Syngnathidae), em laboratório: II. Período juvenil. *Rev. Bras. De Zool.* **2000**, *17*, 515–531. [[CrossRef](#)]
30. Arratia, G.; Schultze, H.P.; Casciotta, J.J. Vertebral column and associated elements in dipnoans and comparison with other fishes: Development and homology. *J. Morphol.* **2001**, *250*, 101–172. [[CrossRef](#)]
31. Bruner, E.; Bartolino, V. Morphological Variation in the Seahorse Vertebral System. *Int. J. Morphol.* **2008**, *26*, 247–262. [[CrossRef](#)]
32. Leysen, H.; Jouk, P.; Brunain, M.; Christiaens, J.; Adriaens, D.J. Cranial architecture of tube-snouted Gasterosteiformes (*Syngnathus rostellatus* and *Hippocampus capensis*). *J. Morphol.* **2010**, *271*, 255–270. [[CrossRef](#)]
33. Leysen, H.; Christiaens, J.; Kegel, B.D.; Boone, M.N.; Hoorebeke, L.V.; Adriaens, D.J. Musculoskeletal structure of the feeding system and implications of snout elongation in *Hippocampus reidi* and *Dunckerocampus dactyliophorus*. *J. Fish Biol.* **2011**, *78*, 1799–1823. [[CrossRef](#)]
34. Novelli, B.; Otero-Ferrer, F.; Socorro, J.A.; Caballero, M.J.; Segade-Botella, A.; Molina Dominguez, L. Development of short-snouted seahorse (*Hippocampus hippocampus*, L. 1758): Osteological and morphological aspects. *Fish Physiol. Biochem.* **2017**, *43*, 833–848. [[CrossRef](#)]
35. Fuiman, L.A. Growth gradients in fish larvae. *J. Fish Biol.* **1983**, *23*, 117–123. [[CrossRef](#)]
36. Mathias, J.A.; Li, S. Feeding Habits of Walleye Larvae and Juveniles: Comparative Laboratory and Field Studies. *Trans. Am. Fish. Soc.* **1982**, *111*, 722–735. [[CrossRef](#)]
37. Franz-Odenaal, T.A.; Adriaens, D. Comparative developmental osteology of the seahorse skeleton reveals heterochrony amongst *Hippocampus* sp. and progressive caudal fin loss. *Evodevo* **2014**, *5*, 45. [[CrossRef](#)] [[PubMed](#)]
38. Bergert, B.A.; Wainwright, P.C.J. Morphology and kinematics of prey capture in the syngnathid fishes *Hippocampus erectus* and *Syngnathus floridae*. *Mar. Biol.* **1997**, *127*, 563–570. [[CrossRef](#)]
39. Choo, C.K.; Liew, H.C. Morphological development and allometric growth patterns in the juvenile seahorse *Hippocampus kuda* Bleeker. *J. Fish Biol.* **2006**, *69*, 426–445. [[CrossRef](#)]
40. Lv, X.; Xu, S.; Liu, Q.; Wang, X.; Yang, J.; Song, Z.; Li, J. Osteological ontogeny and allometric growth in larval and juvenile turbot (*Scophthalmus maximus*). *Aquaculture* **2019**, *498*, 351–363. [[CrossRef](#)]
41. He, T.; Xiao, Z.Z.; Liu, Q.H.; Li, J. Allometric growth in rock bream larvae (Temminck et Schlegel 1844). *J. Fish. China* **2012**, *36*, 1242. [[CrossRef](#)]
42. Osse, J.W.M.; van den Boogaart, J.G.M. Dynamic morphology of fish larvae, structural implications of friction forces in swimming, feeding and ventilation. *J. Fish Biol.* **1999**, *55*, 156–174. [[CrossRef](#)]
43. Gagna, M.R.; Wold, P.A.; Bardal, T.; Øie, G.; Open, E. Allometric growth and development of organs in ballan wrasse (*Labrus bergylta* Ascanius, 1767) larvae in relation to different live prey diets and growth rates. *Biol. Open* **2016**, *5*, 1241–1251. [[CrossRef](#)]
44. Shuiqing, W.U.; Jiaer, L.I.; Youjun, O.U.; Guomin, L.V.; Jianghua, L. Allometric growth of hybrid grouper (*Epinephelus coioides* ♀ × *E. lanceolatus* ♂) larvae and juveniles. *J. Fish. Sci. China* **2014**, *21*, 503–510.
45. Yu-Fu, W.; Zhi-Zhong, X.; Qing-Hua, L.; Jie-Ming, Z.; Zun-Fang, P.; Wen-Hui, M.A.; Dao-Yuan, M.A.; Shi-Hong, X.U.; Yong-Shuang, X.; Jun, L.I.J. Allometric growth pattern during early ontogeny of spotted knifejaw (*Oplegnathus punctatus*). *Mar. Sci.* **2016**, *40*, 43–48.
46. De Lussanet, M.H.; Muller, M. The smaller your mouth, the longer your snout: Predicting the snout length of *Syngnathus acus*, *Centriscus scutatus* and other pipette feeders. *J. R. Soc. Interface* **2007**, *4*, 561–573. [[CrossRef](#)] [[PubMed](#)]
47. Muller, M. Optimization principles applied to the mechanism of neurocranium levation and mouth bottom depression in bony fishes (Halecostomi). *J. Theor. Biol.* **1987**, *126*, 343–368. [[CrossRef](#)]
48. Detwyler, R.; Houde, E.D. Food selection by laboratory-reared larvae of the scaled sardine *Harengula pensacolatae* (Pisces, Clupeidae) and the bay anchovy *Anchoa mitchilli* (Pisces, Engraulidae). *Mar. Biol.* **1970**, *7*, 214–222. [[CrossRef](#)]
49. Teixeira, R.L.; Musick, J.A. Trophic ecology of two congeneric pipefishes (Syngnathidae) of the lower York River, Virginia. *Environ. Biol. Fishes* **1995**, *43*, 295–309. [[CrossRef](#)]
50. Porter, M.M.; Adriaens, D.; Hatton, R.L.; Meyers, M.A.; McKittrick, J. BIOMECHANICS. Why the seahorse tail is square. *Science* **2015**, *349*, aaa6683. [[CrossRef](#)]

51. Praet, T.; Adriaens, D.; Cauter, S.V.; BertMasschaele; Beule, M.D.; Verhegghe, B. Inspiration from nature: Dynamic modelling of the musculoskeletal structure of the seahorse tail. *Int. J. Numer. Methods Biomed. Eng.* **2012**, *28*, 1028. [[CrossRef](#)]
52. Porter, M.M.; Novitskaya, E.; Castro-Cesena, A.B.; Meyers, M.A.; McKittrick, J. Highly deformable bones: Unusual deformation mechanisms of seahorse armor. *Acta Biomater* **2013**, *9*, 6763–6770. [[CrossRef](#)]

Disclaimer/Publisher’s Note: The statements, opinions and data contained in all publications are solely those of the individual author(s) and contributor(s) and not of MDPI and/or the editor(s). MDPI and/or the editor(s) disclaim responsibility for any injury to people or property resulting from any ideas, methods, instructions or products referred to in the content.